Electronic Supplementary Material (ESI) for Green Chemistry.

Supporting Information

Stabilising Ni catalysts for the dehydration-decarboxylation-hydrogenation of citric acid to methylsuccinic acid

Jasper Verduyckt,[a] Anton Geers,[a] Birgit Claes,[a] Samuel Eyley,[b] Cédric Van Goethem,[a] Ivo Stassen,[a] Simon Smolders,[a] Rob Ameloot,[a] Ivo Vankelecom,[a] Wim Thielemans,[b] and Dirk E. De Vos [a]*

[a] *Centre for Surface Chemistry and Catalysis, Department of Microbial and Molecular Systems, KU Leuven – University of Leuven, Leuven Chem&Tech, Celestijnenlaan 200F, Post Box 2461, 3001 Heverlee, Belgium*

[b] *Renewable Materials and Nanotechnology Research Group, Department of Chemical Engineering, KU Leuven – University of Leuven, Campus Kulak Kortrijk, Etienne Sabbelaan 53, 8500 Kortrijk, Belgium*

* E-mail: dirk.devos@kuleuven.be

1. Experimental details

1.1. Materials

All chemicals were used as received: citric acid monohydrate (Sigma-Aldrich, ≥99.5%), *trans*-aconitic acid (Sigma-Aldrich, 98%), mesaconic acid (Sigma-Aldrich, 99%), itaconic acid (TCI, >99.0%), methacrylic acid (Acros Organics, 99.5%), NaOH (Fischer Scientific, 99.1%), KOH (Acros Organics, 85%), nickel(II)sulphate hexahydrate (Sigma-Aldrich, >99%), nickel(II)nitrate hexahydrate (Fluka, >98.5%), nickel(II)acetate tetrahydrate (Janssen Chimica, >99%), iron(III)nitrate nonahydrate (ABCR, 98%), iron(II)acetate (Acros Organics, 95%), iron(0) powder (Sigma-Aldrich, 97%), N_2 (Air Liquide, α1), H_2 (Air Liquide, N40), dilute O_2 in N_2 (Air Liquide, 1%), Ni/SiO_2 (64 wt%, Strem Chemicals), Ni/SiO_2-Al_2O_3 (65 wt%, Sigma-Aldrich), HTC Ni 500 RP 1.2mm (Johnson Matthey), Katalco JM 11-4R (Johnson Matthey), Katalco JM 23-8 (Johnson Matthey), Ni-C NPs (96.39 wt%, US Research Nanomaterials), $MgAl_2O_4$ (Sigma-Aldrich), ZrO_2 (Alfa Aesar), TiO_2 (Alfa Aesar), Al_2O_3 (Condea Chemie, Puralox NGa-150), benzyl alcohol (Sigma-Aldrich, 99+%) and D_2O (Sigma-Aldrich, 99.9% D).

1.2. Catalyst synthesis

Conventional Ni catalysts (5 wt%) supported on $MgAl_2O_4$, Al_2O_3, ZrO_2 and TiO_2 were synthesised by incipient wetness impregnation. In a typical procedure 2 g of support was impregnated with a solution of $Ni(NO_3)_2$ in deionised water. Impregnated supports were then dried overnight at 60°C, granulated to particles with sizes between 250 and 500 µm, followed by reduction (1 h, T, 2°C/min, 150 mL/min H_2) and passivation (1 h, RT, 50 mL/min 1% O_2 in N_2). The reduction temperature was dependent on the support material and was determined from temperature-programmed reduction (TPR) profiles found in literature: 800°C, 800°C, 650°C and 500°C for $MgAl_2O_4$, Al_2O_3, ZrO_2 and TiO_2, respectively.[1-4]

NiFe/ZrO_2 catalysts (5 wt% Ni; 1, 3 or 5 wt% Fe) were also synthesised by incipient wetness impregnation. 2 g of ZrO_2 was co-impregnated with a solution of $Ni(NO_3)_2$ and $Fe(NO_3)_3$ in deionised water. Impregnated supports were then dried overnight at 60°C, granulated to particles with sizes between 250 and 500 µm, followed by reduction (1 h, 650°C, 2°C/min, 150 mL/min H_2) and passivation (1 h, RT, 50 mL/min 1% O_2 in N_2). The Fe/ZrO_2 catalyst was prepared in the same way, without the addition of $Ni(NO_3)_2$.

On the other hand, Ni_5Fe_5/ZrO_2 (Ac) (5 wt% Ni, 5 wt% Fe) was prepared via wet impregnation. 2 g of ZrO_2 was added to an aqueous solution (20 mL deionised water) containing $Ni(CH_3COO)_2$ and $Fe(CH_3COO)_2$. This solution was stirred at room temperature until the water was completely evaporated. The impregnated supports were further dried overnight at 60°C, granulated to particles with sizes between 250 and 500 µm, followed by reduction (1 h, 650°C, 2°C/min, 150 mL/min H_2) and passivation (1 h, RT, 50 mL/min 1% O_2 in N_2).

1.3. Catalyst characterisation

Possible Ni and Fe leaching was measured by ICP-OES at 231.60 nm and 238.20 nm, respectively, using a Varian 720-ES with the Varian SPS3 sample preparation system and applying the calibration curve method. 100 µL of the supernatant of the reaction mixture was diluted with 9.9 mL of 0.42 N HNO_3 in Milli-Q water. N_2 physisorption measurements were performed using a Micromeritics 3Flex surface analyser at -196°C. Before the measurements, the 100 mg (or 500 mg in the case of the Ni-C NPs) samples were outgassed at 150°C for 6 h under vacuum. Powder XRD patterns were recorded with a STOE Stadi P HT diffractometer using Cu K_α-radiation. TEM specimens were prepared by depositing the catalyst particles on a Lacey carbon-coated TEM grid (300 mesh Cu grid, Pacific Grid Tech, USA). TEM and STEM images, and EDX elemental maps were collected utilising a JEOL ARM200F TEM operated at 200 kV, and equipped with a cold FEG and a probe aberration corrector. XPS spectra were recorded on a Kratos Axis Supra X-ray Photoelectron Spectrometer employing a monochromated Al K_α ($h\upsilon$ = 1486.6 eV, 300 W) X-ray source, hybrid (magnetic/electrostatic) optics (slot aperture), hemispherical analyser, multichannel plate and delay line detector (DLD) with a take-off angle of 90° and an acceptance angle of 30°. The analyser was operated in fixed analyser transmission (FAT) mode with survey scans taken with a pass energy of 160 eV and high resolution scans with a pass energy of 20 eV. All scans were acquired under charge neutralisation conditions using a low energy electron gun within the field of the magnetic lens. The resulting spectra were processed using CasaXPS software. Binding energy was referenced to aliphatic adventitious carbon at 284.8 eV for Ni/ZrO_2 and Ni_5Fe_5/ZrO_2, and to graphitic carbon at 284.4 eV for the Ni-C NPs.[5] Ni $2p_{3/2}$ spectra were fitted with component peaks based on the work of Biesinger *et al.* for the quantification of mixed Ni, Ni oxide and Ni hydroxide systems.[6] Relative intensities, full widths at half maxima (FWHM) and peak separations were fixed for the different species. The scale, binding energy and FWHM of the populations of peaks were parametrised during the fit to determine the relative concentrations of each species.

1.4. Catalytic reaction

In a typical reaction a solution of citric acid in deionised water (2 mL, 0.1 M), a catalyst (10 mol% Ni-C NPs) and a magnetic stirring bar were loaded into a teflon-lined stainless steel reactor (4.3 mL). Next, the reactor was sealed and the atmosphere was flushed six times with N_2. Then, after pressurizing the reactor with 2 bar N_2 followed by 30 bar H_2, the mixture was magnetically stirred at 500 rpm and heated to 175°C. After 6 h the reaction was quenched by cooling with water and ice. Afterwards, the catalyst was separated from the solution by centrifugation. The industrial Johnson Matthey catalysts were ground to a fine powder before use. For recycling experiments the teflon liner was drawn from the stainless steel reactor and the Ni-C NPs were magnetically separated from the solution in the liner. Subsequently the solution was decanted, after which the liner was re-inserted in the reactor. Then, 2 mL of the citric acid solution was added again, the reactor was sealed and the reaction progressed as described at the beginning of this paragraph.

1.5. Product analysis and identification

To determine the conversion of citric acid and the selectivities to the different products, the reaction mixtures were analysed by ^{1}H-NMR. Samples were prepared by adding 300 µL of the reaction mixture to 300 µL of D_2O containing an external standard (benzyl alcohol, 0.1 M). ^{1}H-; ^{1}H,^{1}H-COSY-; ^{1}H,^{13}C-HSQC- and ^{1}H,^{13}C-HMBC-NMR spectra were recorded on a Bruker Ascend 400 MHz spectrometer equipped with a BBO 5 mm atma probe and a sample case. The broad signal of water in the ^{1}H-NMR spectra was suppressed by applying an adapted zgpr pulse program: p1 9.75 µs; plw1 15W; plw9 5.7-05W; o1P on the resonance signal of water, determined and selected automatically.

The different selectivities (*S*) mentioned in the paper were calculated as follows:

$$S_{MSA} = \frac{Y_{MSA}}{X}$$

$$S_{2^{nd}\ deca} = \frac{Y_{MAA} + Y_{BA} + Y_{IBA} + Y_{HIBA}}{X}$$

$$S_{Fragmentation} = \frac{Y_{Ac} + Y_{AA}}{X}$$

$$S_{Itaconic\ isomers} = \frac{Y_{IA} + Y_{MA} + Y_{CA}}{X}$$

$$S_{Isomer\ hydration} = \frac{Y_{HMSA} + Y_{CBL} + Y_{H2MSA}}{X}$$

Where MSA, MAA, BA, IBA, HIBA, Ac, AA, IA, MA, CA, HMSA, CBL and H2MSA stand for methylsuccinic acid, methacrylic acid, butyric acid, isobutyric acid, 2-hydroxyisobutyric acid, acetone, acetic acid, itaconic acid, mesaconic acid, citraconic acid, 2-(hydroxymethyl)succinic acid, β-carboxy-γ-butyrolactone and 2-hydroxy-2-methylsuccinic acid, respectively. Pyruvic and lactic acid were not considered in the calculation of the selectivity for fragmentation products, since these compounds originate from the same citric acid molecule as acetic acid.[7] *Y* = yield and *X* = conversion, always on a molar basis.

2. N_2 physisorption data of Ni/ZrO_2 and Ni_5Fe_5/ZrO_2

Table S1. Textural properties of Ni/ZrO_2 and Ni_5Fe_5/ZrO_2.

Catalyst	S [m²/g] [a]	V [cm³/g] [b]	d [nm] [c]
Ni/ZrO_2	52	0.21	13
Ni_5Fe_5/ZrO_2	44	0.20	14

[a] BET surface area. [b] BJH pore volume derived from desorption isotherm. [c] BJH average pore diameter derived from desorption isotherm.

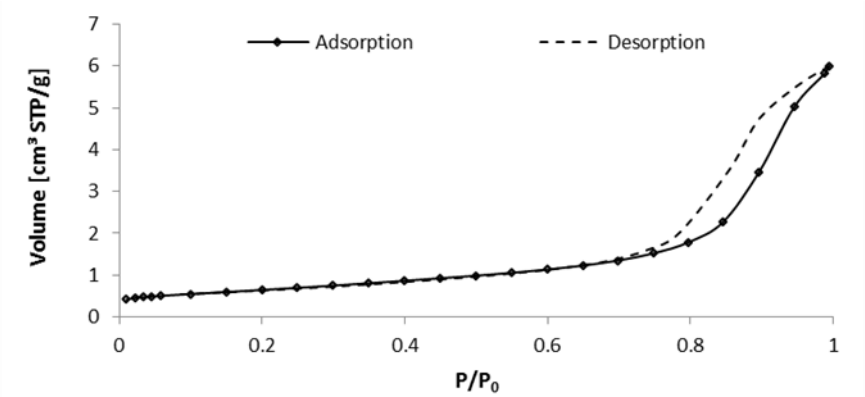

Figure S1. N_2 physisorption isotherms of Ni/ZrO_2.

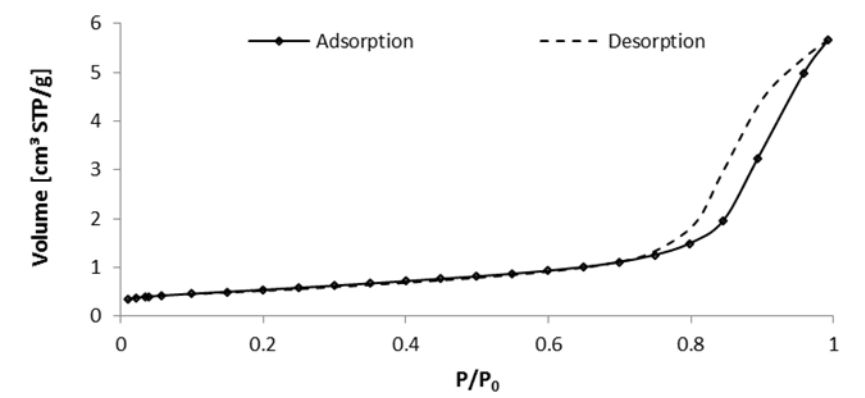

Figure S2. N_2 physisorption isotherms of Ni_5Fe_5/ZrO_2.

3. XRD data of Ni/ZrO_2 and Ni_5Fe_5/ZrO_2

The X-ray diffractograms of Ni/ZrO_2 and Ni_5Fe_5/ZrO_2 were compared to the diffractogram of bare ZrO_2 (**Figure S3**). No metal peaks could be distinguished; one can only conclude that the support remained stable during the catalyst synthesis procedure.

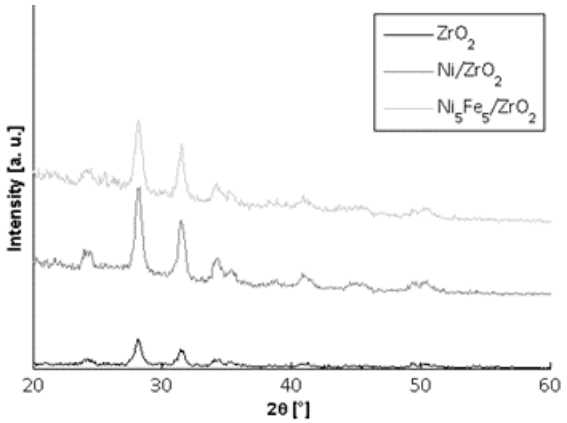

Figure S3. X-ray diffractograms of ZrO_2, Ni/ZrO_2 and Ni_5Fe_5/ZrO_2.

4. XPS data

4.1. Ni/ZrO_2

Data obtained from the XPS spectra regarding the elemental composition of the Ni/ZrO_2 sample, are displayed in **Table S2**. The wide scan shows 5 at% Ni in the sample corresponding to 7.1% by mass. The fitting of the Ni $2p_{3/2}$ peak (**Figure S4**) shows three populations of peaks corresponding with Ni metal (0.4%), Ni(II)oxide (46.4%) and Ni(II)hydroxide (53.2%).

Table S2. XPS data for Ni/ZrO_2.

Orbital	Component	Binding Energy /eV	FWHM /eV	Rel. A /%[a]	At %
Ni $2p_{3/2}$	Ni	852.6	0.88	0.36	0.02
	Ni	856.2	2.50	0.03	0.00
	Ni	858.6	2.50	0.05	0.00
	NiO	853.8	1.57	6.62	0.33
	NiO	855.5	4.99	20.48	1.02
	NiO	861.0	5.77	15.77	0.79
	NiO	864.1	3.13	1.67	0.08
	NiO	866.4	3.75	1.81	0.09
	$Ni(OH)_2$	855.0	1.23	3.93	0.20
	$Ni(OH)_2$	855.7	2.43	24.09	1.20
	$Ni(OH)_2$	857.8	1.69	1.60	0.08
	$Ni(OH)_2$	860.6	1.12	0.75	0.04
	$Ni(OH)_2$	861.6	4.93	20.87	1.04
	$Ni(OH)_2$	866.5	3.19	1.97	0.10
	All			100	5.00
O 1s		529.5	1.91	71.20	42.72
		531.3	1.91	28.80	17.28
	All			100	60.00
C 1s	C-C	284.8	2.42	76.09	3.25
	O-C=O[8]	288.5	2.42	23.91	1.02
	All			100	4.27
Zr 3d	$j = 5/2$	181.2	1.49	59.00	18.14
	$j = 3/2$	183.6	1.49	41.00	12.60
	All			100	30.74

[a] Area relative to other components of same orbital

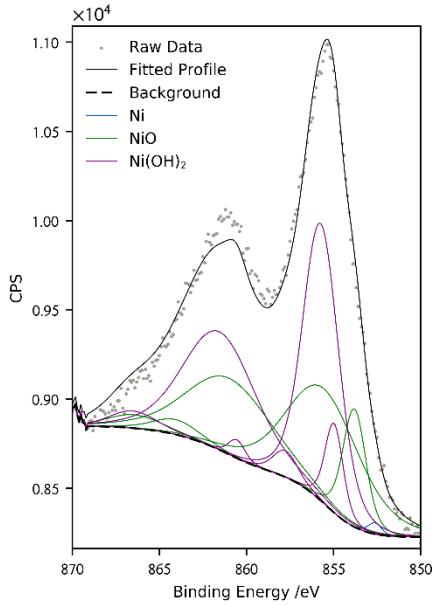

Figure S4. Ni 2p high resolution spectrum of Ni/ZrO_2.

4.2. Ni_5Fe_5/ZrO_2

XPS data for the Ni_5Fe_5/ZrO_2 sample are presented in **Table S3**. Analysis of the Ni $2p_{3/2}$ high resolution scan (**Figure S5**) shows three populations of peaks corresponding with Ni metal (3.7%), Ni(II)oxide (48.8%) and Ni(II)hydroxide (47.6%). Unfortunately, quantification of Fe in this sample was not possible due to overlap between the Fe 2p doublet and Ni LMM Auger peaks. Other Fe transitions (3p and 3s) were too weak to be detected. The lack of data for Fe should be taken into account when considering atomic concentrations presented here. Despite this difficulty, the binding energy of the Fe $2p_{3/2}$ peak was determined from the high resolution scan (**Figure S6**) to be 711.0 eV, corresponding to an Fe(III) species – presumably Fe(III)oxide in this case.[9]

Table S3. XPS data for Ni_5Fe_5/ZrO_2.

Orbital	Component	Binding Energy /eV	FWHM /eV	Rel. A /%[a]	At %
Na 1s[b]		1071.5	2.5	100	0.55
Ni $2p_{3/2}$	Ni	852.3	1.46	2.97	0.06
	Ni	856.0	4.15	0.23	0.00
	Ni	858.3	4.15	0.46	0.01
	NiO	854.0	1.80	6.97	0.13
	NiO	855.7	5.73	21.55	0.40
	NiO	861.2	6.63	16.59	0.31
	NiO	864.3	3.60	1.76	0.03
	NiO	866.6	4.30	1.91	0.04
	$Ni(OH)_2$	854.9	1.32	3.52	0.07
	$Ni(OH)_2$	855.7	2.61	21.54	0.40
	$Ni(OH)_2$	857.7	1.81	1.43	0.03
	$Ni(OH)_2$	860.5	1.21	0.67	0.01
	$Ni(OH)_2$	861.5	5.29	18.66	0.35
	$Ni(OH)_2$	866.4	3.42	1.76	0.03
	All			100	1.87
Fe 2p[c]	$j = 3/2$	711.0	4.13	66.62	-
	$j = 1/2$	724.1	4.13	33.38	-
	All			100	-
O 1s		529.5	1.83	77.83	46.34
		531.2	1.83	22.17	13.20
	All			100	59.54
C 1s	C-C	284.8	2.23	77.86	4.20
	O-C=O [8]	288.8	2.23	22.14	1.19
	All			100	5.39
Zr 3d	$j = 5/2$	181.5	1.59	58.61	19.14
	$j = 3/2$	183.8	1.59	41.39	13.52
	All			100	32.66

[a] Area relative to other components of same orbital
[b] Taken from wide scan data
[c] Area and relative separation fixed to reflect spin-orbit splitting[10]

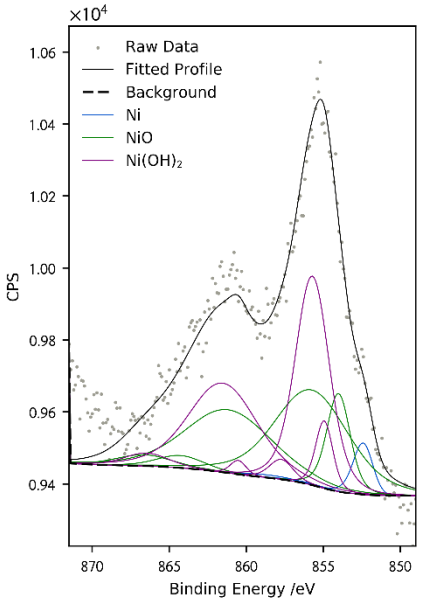

Figure S5. Ni 2p high resolution spectrum of Ni_5Fe_5/ZrO_2.

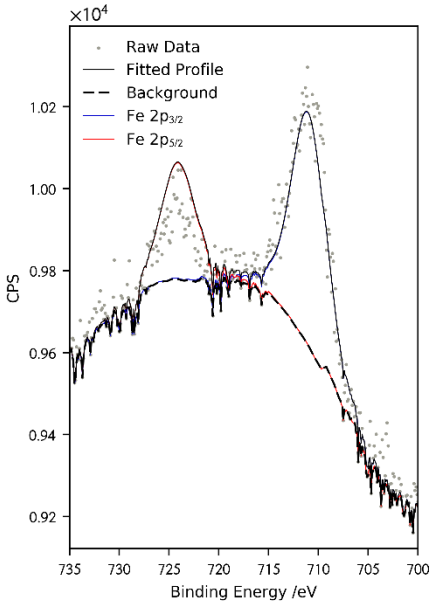

Figure S6. Fe 2p high resolution spectrum of Ni_5Fe_5/ZrO_2.

4.3. Ni-C NPs

XPS data for the Ni-C NPs are presented in **Table S4**. Analysis of the nickel $2p_{3/2}$ spectrum (**Figure S7**) shows only presence of Ni metal. Although relative intensities of the component peaks for Ni metal do not match with the literature values, analysis of the O 1s binding energy shows the lack of metal oxide species in this sample.[11] The C 1s spectrum for this material (**Figure S8**) is highly asymmetric, which is typical of sp^2 hybridised carbon. The main C 1s peak was assigned to 284.4 eV, corresponding with graphitic carbon.[5] This assignment was justified via comparison of the metallic Ni $2p_{3/2}$ binding energy of 852.5 eV with the literature value of 852.6 eV.[6] Two further component peaks are assigned, one to oxidised carbon species at 288.0 eV and one to plasmon losses. The presence of two peaks in the O 1s spectrum suggests multiple oxidised species, but plasmon losses obscure this area of the C 1s spectrum.

Table S4. XPS data for the Ni-C NPs.

Orbital	Component	Binding Energy /eV	FWHM /eV	Rel. A /%[a]	At %
Ni $2p_{3/2}$	Ni	852.5	0.97	72.00	23.42
	Ni	856.1	2.77	10.67	3.47
	Ni	858.5	2.77	17.34	5.64
	All			100	32.53
O 1s		531.5	1.83	77.83	1.70
		533.1	1.83	22.17	0.27
	All			100	1.97
C 1s	Graphitic	284.4	0.86	85.17	55.79
	C=O	288.0	3.21	5.61	3.67
	Plasmon	290.7	3.51	9.22	6.04
	All			100	65.50

[a] Area relative to other components of same orbital

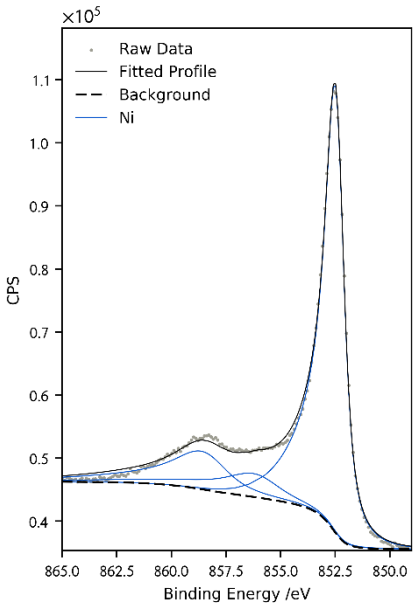

Figure S7. Ni 2p high resolution spectrum of the Ni-C NPs.

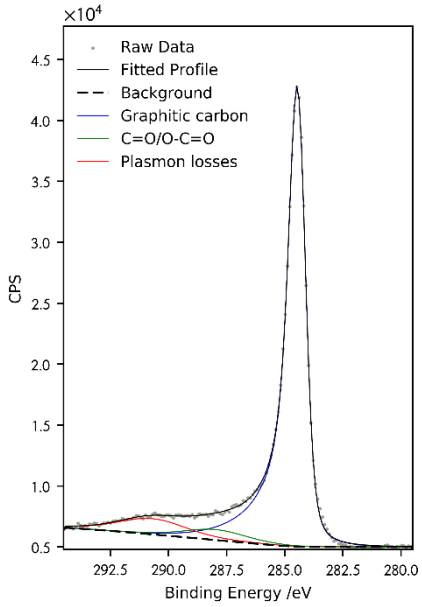

Figure S8. C 1s high resolution spectrum of the Ni-C NPs.

5. N_2 physisorption data of the Ni-C NPs

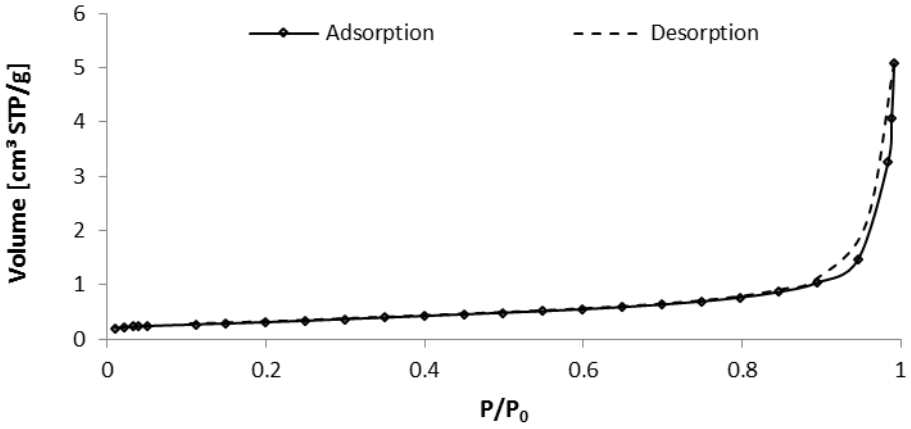

Figure S9. N_2 physisorption isotherms of the Ni-C NPs.

6. Recycling experiments

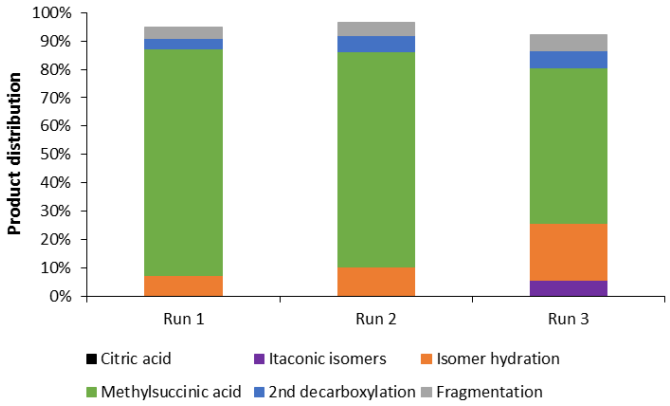

Figure S10. Recycling experiments. Reaction conditions: citric acid (0.2 mmol), Ni-C NPs (20 mol% Ni), water (2 mL), 175°C, 2 bar N_2 and 30 bar H_2, 6 h.

7. Product identification

General information: ^{1}H-NMR spectra were calibrated by setting the singlet signal of the external standard (benzyl alcohol) to 4.65 ppm.[12]

Citric acid (MW = 192 g/mol)

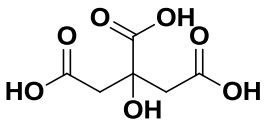

^{1}H-NMR (400 MHz, H_2O/D_2O): δ (ppm) = 3.03 (d, 2H, -C**H**$_2$-COOH), 2.85 (d, 2H, -C**H**$_2$-COOH).

Itaconic acid (MW = 130 g/mol)

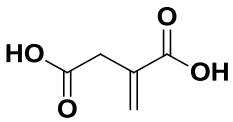

^{1}H-NMR (400 MHz, H_2O/D_2O): δ (ppm) = 6.38 (s, 1H, C**H**$_2$=C(COOH)-), 5.90 (s, 1H, C**H**$_2$=C(COOH)-), 3.43 (s, 2H, -C**H**$_2$-COOH).

^{13}C{^{1}H}-NMR (400 MHz, H_2O/D_2O): δ (ppm) = 175.4 (1C, -CH$_2$-**C**OOH), 169.5 (1C, CH$_2$=C(**C**OOH)-), 133.2 (1C, CH$_2$=**C**<), 130.2 (1C, **C**H$_2$=C<), 36.9 (1C, -**C**H$_2$-COOH).

Mesaconic acid (MW = 130 g/mol)

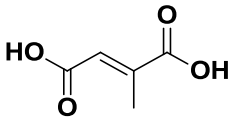

^{1}H-NMR (400 MHz, H_2O/D_2O): δ (ppm) = 6.78 (s, 1H, =C**H**-COOH), 2.14 (s, 3H, C**H$_3$**-C(COOH)=).
^{13}C{^{1}H}-NMR (400 MHz, H_2O/D_2O): δ (ppm) = 171.3 (1C, CH_3-C(**C**OOH)=), 142.7 (1C, -CH=**C**<), 127.3 (1C, -**C**H=C<), 14.2 (1C, ≥C-**C**H$_3$). The other carboxylic acid carbon could not be observed via HSQC, nor HMBC.

Citraconic acid (MW = 130 g/mol)

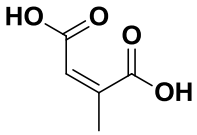

^{1}H-NMR (400 MHz, H_2O/D_2O): δ (ppm) = 5.95 (s, 1H, =C**H**-COOH), 2.04 (s, 3H, C**H$_3$**-C(COOH)=).
^{13}C{^{1}H}-NMR (400 MHz, H_2O/D_2O): δ (ppm) = 174.8 (1C, CH_3-C(**C**OOH)=), 149.3 (1C, -CH=**C**<), 120.1 (1C, -**C**H=C<), 21.1 (1C, ≥C-**C**H$_3$). The other carboxylic acid carbon could not be observed via HSQC, nor HMBC.

Methylsuccinic acid (MW = 132 g/mol)

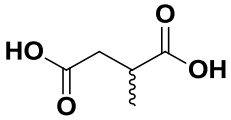

^{1}H-NMR (400 MHz, H_2O/D_2O): δ (ppm) = 2.97-2.84 (m, 1H, -C**H**(CH_3)-COOH), 2.70 (dd, 1H, -C**H$_2$**-COOH), 2.58 (dd, 1H, -C**H$_2$**-COOH), 1.21 (d, 3H, -CH(C**H$_3$**)-COOH).
^{13}C{^{1}H}-NMR (400 MHz, H_2O/D_2O): δ (ppm) = 180.2 (1C, -CH(CH_3)-**C**OOH), 176.6 (1C, -CH_2-**C**OOH), 36.9 (1C, -**C**H$_2$-COOH), 35.7 (1C, -**C**H(CH_3)-COOH), 16.1 (1C, -CH(**C**H$_3$)-COOH).

Methacrylic acid (MW = 86 g/mol)

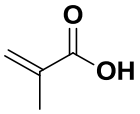

^{1}H-NMR (400 MHz, H_2O/D_2O): δ (ppm) = 6.10 (s, 1H, C**H$_2$**=C(COOH)-), 5.72 (s, 1H, C**H$_2$**=C(COOH)-), 1.91 (s, 3H, C**H$_3$**-C(=CH_2)-).
^{13}C{^{1}H}-NMR (400 MHz, H_2O/D_2O): δ (ppm) = 171.3 (1C, -**C**OOH), 136.2 (1C, CH_2=**C**<), 126.7 (1C, **C**H$_2$=C<), 17.5 (1C, ≥C-**C**H$_3$).

Isobutyric acid (MW = 88 g/mol)

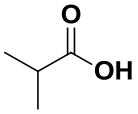

^{1}H-NMR (400 MHz, H_2O/D_2O): δ (ppm) = 2.60 (hp, 1H, -C**H**$(CH_3)_2$), 1.14 (d, 6H, -CH(C**H$_3$**$)_2$).
^{13}C{^{1}H}-NMR (400 MHz, H_2O/D_2O): δ (ppm) = 182.6 (1C, >CH-**C**OOH), 33.9 (1C, -**C**H$(CH_3)_2$), 17.8 (2C, -CH(**C**$H_3)_2$).

Butyric acid (MW = 88 g/mol)

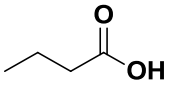

^{1}H-NMR (400 MHz, H_2O/D_2O): δ (ppm) = 2.36 (t, 2H, -C**H$_2$**-COOH), 1.61 (sx, 2H, CH_3-C**H$_2$**-CH_2-), 0.93 (t, 3H, C**H$_3$**-CH_2-).

Acetone (MW = 58 g/mol)

^{1}H-NMR (400 MHz, H_2O/D_2O): δ (ppm) = 2.23 (s, 6H, C**H$_3$**-).
^{13}C{^{1}H}-NMR (400 MHz, H_2O/D_2O): δ (ppm) = 30.2 (2C, **C**H_3-). Carbonyl carbon could not be observed via HSQC, nor HMBC.

Acetic acid (MW = 60 g/mol)

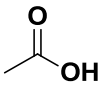

^{1}H-NMR (400 MHz, H_2O/D_2O): δ (ppm) = 2.10 (s, 3H, C**H$_3$**-).
^{13}C{^{1}H}-NMR (400 MHz, H_2O/D_2O): δ (ppm) = 176.6 (1C, -**C**OOH), 20.6 (1C, **C**H_3-).

Pyruvic acid (MW = 88 g/mol)

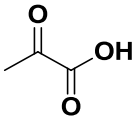

^{1}H-NMR (400 MHz, H_2O/D_2O): δ (ppm) = 2.38 (s, 3H, C**H$_3$**-).

Lactic acid (MW = 90 g/mol)

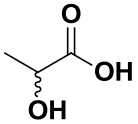

^{1}H-NMR (400 MHz, H_2O/D_2O): δ (ppm) = 4.39 (q, 1H, CH_3-C**H**(OH)-), 1.43 (d, 3H, C**H$_3$**-CH(OH)-).
^{13}C{^{1}H}-NMR (400 MHz, H_2O/D_2O): δ (ppm) = 178.4 (1C, -**C**OOH), 66.0 (1C, -**C**H(OH)-), 19.3 (1C, **C**H_3-).

2-Hydroxyisobutyric acid (MW = 104 g/mol)

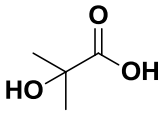

^{1}H-NMR (400 MHz, H_2O/D_2O): δ (ppm) = 1.46 (s, 6H, C**H**$_3$-).
^{13}C{^{1}H}-NMR (400 MHz, H_2O/D_2O): δ (ppm) = 180.2 (1C, -**C**OOH), 72.6 (1C, -**C**(OH)<$(CH_3)_2$), 26.2 (2C, **C**H_3-).

β-Carboxy-γ-butyrolactone (MW = 130 g/mol)

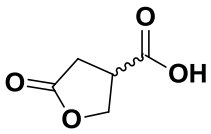

^{1}H-NMR (400 MHz, H_2O/D_2O): δ (ppm) = 4.64 (dd, 1H, -O-C**H**$_2$-CH<), 4.59 (dd, 1H, -O-C**H**$_2$-CH<), 3.66-3.57 (m, 1H, -CH_2-C**H**(COOH)-CH_2-), 2.94-2.88 (m, 2H, -C(=O)-C**H$_2$**-CH<).
^{13}C{^{1}H}-NMR (400 MHz, H_2O/D_2O): δ (ppm) = 179.6 (1C, >CH-**C**OOH), 176.0 (1C, -O-**C**(=O)-CH_2-), 70.2 (1C, -O-**C**H_2-CH<), 39.8 (1C, -CH_2-**C**H(COOH)-CH_2-), 30.9 (1C, -C(=O)-**C**H_2-CH<).

2-(Hydroxymethyl)succinic acid (MW = 148 g/mol)

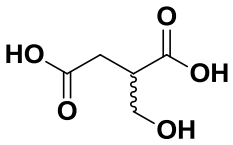

^{1}H-NMR (400 MHz, H_2O/D_2O): δ (ppm) = 3.86 (dd, 1H, HO-C**H**$_2$-CH<), 3.79 (dd, 1H, HO-C**H**$_2$-CH<), 3.06-2.99 (m, 1H, -CH_2-C**H**(COOH)-CH_2-), 2.78 (dd, 1H, -C**H**$_2$-COOH), 2.63 (dd, 1H, -C**H**$_2$-COOH).
^{13}C{^{1}H}-NMR (400 MHz, H_2O/D_2O): δ (ppm) = 177.2 (1C, >CH-**C**OOH), 61.8 (1C, HO-**C**H_2-CH<), 32.1 (1C, -**C**H_2-COOH). The other carbons could not be observed via HSQC, nor HMBC.

2-Hydroxy-2-methylsuccinic acid (MW = 148 g/mol)

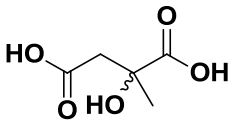

^{1}H-NMR (400 MHz, H_2O/D_2O): δ (ppm) = 3.09 (d, 1H, -C**H**$_2$-COOH), 2.75 (d, 1H, -C**H**$_2$-COOH), 1.49 (s, 3H, -C**H$_3$**).
^{13}C{^{1}H}-NMR (400 MHz, H_2O/D_2O): δ (ppm) = 179.0 (1C, >C(OH)-**C**OOH), 174.3 (1C, -CH_2-**C**OOH), 72.0 (1C, >**C**(OH)-COOH), 43.4 (1C, -**C**H_2-COOH), 25.6 (1C, -**C**H_3).

8. References

(1) Z. Mosayebi, M. Rezaei, A. B. Ravandi and N. Hadian*, Int. J. Hydrogen Energy,* 2012, **37,** 1236–1242.

(2) R. Wang, Y. Li, R. Shi and M. Yang, *J. Mol. Catal. A: Chem.,* 2011, **344,** 122–127.

(3) M. Rezaei, S. M. Alavi, S. Sahebdelfar and Z.-F. Yan, *Mater. Lett.,* 2007, **61,** 2628–2631.

(4) S. Chettibi, N. Keghouche, Y. Benguedouar, M. M. Bettahar and J. Belloni, *Catal. Lett.,* 2013, **143,** 1166–1174.

(5) Y. Mizokawa, T. Miyasato, S. Nakamura, K. M. Geib and C. W. Wilmsen, *J. Vac. Sci. Technol., A,* 1987, **5,** 2809–2813.

(6) M. C. Biesinger, B. P. Payne, L. W. M. Lau, A. R. Gerson and R. S. C. Smart, *Surf. Interface Anal.,* 2009, **41,** 324–332.

(7) J. Verduyckt and D. E. De Vos, *Chem. Sci.,* 2017, **8,** 2616–2620.

(8) Thermo Fisher Scientific, http://xpssimplified.com/elements/carbon.php, accessed May, 2017.

(9) M. C. Biesinger, B. P. Payne, A. P. Grosvenor, L. W. M. Lau, A. R. Gerson and R. S. C. Smart, *Appl. Surf. Sci.,* 2011, **257,** 2717–2730.

(10) Thermo Fisher Scientific, http://xpssimplified.com/elements/iron.php, accessed May, 2017.

(11) Thermo Fisher Scientific, http://xpssimplified.com/elements/oxygen.php, accessed May, 2017.

(12) N. R. Babij, E. O. McCusker, G. T. Whiteker, B. Canturk, N. Choy, L. C. Creemer, C. V. De Amicis, N. M. Hewlett, P. L. Johnson, J. A. Knobelsdorf, F. Li, B. A. Lorsbach, B. M. Nugent, S. J. Ryan, M. R. Smith and Q. Yang, *Org. Process Res. Dev.,* 2016, **20,** 661–667.